Magnetic instabilities in doped Fe_2YZ full-Heusler thermoelectric compounds

Sébastien Lemal,[1,*] Fabio Ricci,[1,*] Daniel I. Bilc,[2] Matthieu J. Verstraete,[3] and Philippe Ghosez[1]

[1] *Theoretical Materials Physics, Q-Mat, CESAM, Université de Liège, B-4000 Liège, Belgium*
[2] *Faculty of Physics, Babeş-Bolyai University, 1 Kogălniceanu, 400084 Cluj-Napoca, Romania*
[3] *Nanomat, Q-Mat, CESAM and European Theoretical Spectroscopy Facility, Université de Liège, B-4000 Liège, Belgium*

(Dated: October 15, 2019)

Thermoelectricity is a promising avenue for harvesting energy but large-scale applications are still hampered by the lack of highly-efficient low-cost materials. Recently, Fe_2YZ Heusler compounds were predicted theoretically to be interesting candidates with large thermoelectric power factor. Here, we show that under doping conditions compatible with thermoelectric applications, these materials are prone to an unexpected magnetic instability detrimental to their thermoelectric performance. We rationalize the physics at the origin of this instability, provide guidelines for avoiding it and discuss its impact on the thermoelectric power factor. Doing so, we also point out the shortcomings of the rigid band approximation commonly used in high-throughput theoretical searches of new thermoelectrics.

Thermoelectric (TE) modules realizing the direct conversion of wasted heat into electricity appear as very promising devices for clean energy harvesting [1]. However, concrete TE applications still remain limited to niche markets due to the lack of cheap and efficient thermoelectric compounds. The efficiency of thermoelectrics is quantified by their figure of merit $ZT = S^2\sigma T/\kappa$ involving the Seebeck coefficient (S), the electrical conductivity (σ), the temperature (T) and the thermal conductivity (κ). Attempts to optimize ZT by reducing κ already led to record values in Bi_2Te_3 ($\sim$2.4) [2] and SnSe ($\sim$2.6) based systems [3]. Further improvements now imply also boosting the power factor (PF), $S^2\sigma$, using nontrivial electronic band structure engineering. The simultaneous increase of S and σ is challenging as it requires mutually exclusive characteristics [4]: abruptly changing density of states (flat bands) and large group velocity (dispersive bands).

The fast screening of the PF of a vast palette of compounds using computational methods appears as a very useful approach in order to identify new promising TE candidates with suitable performance [5–7]. This screening typically relies on first-principles calculations of the electronic properties of pristine phases, and the use of the rigid band approximation to predict the TE properties under appropriate doping [6, 8]. Using such an approach, Bilc *et al.* [9] recently identified Fe_2YZ full Heusler compounds as a new class of attractive candidates with large PF. The interesting properties of Fe_2YZ compounds were linked to the highly-directional character of the Fe 3d states, leading to "flat-and-dispersive" bands compatible with Mahan's requirements [4].

In this Letter, we study from first-principles the properties of Fe_2YZ compounds under explicit doping, and show that they are prone to a magnetic instability which is detrimental to their TE properties. We rationalize the origin of this instability and provide guiding rules for avoiding it. Our work confirms the interest of Fe_2YZ compounds for TE applications, further extending it to thermo-magnetic applications. We also demonstrate that theoretical predictions based on the rigid band approximation in the pristine phase can often be qualitatively incorrect, and should be more systematically complemented by simulations under explicit doping.

Methods. Density Functional Theory (DFT) simulations are performed using the CRYSTAL [10, 11] and ABINIT [12] codes. With CRYSTAL, we performed hybrid functional calculations relying on the B1 Wu-Cohen [13] (B1-WC) functional, previously used for this class of materials [9]. With ABINIT, we used the Projector Augmented Wave method, and the Generalized Gradient Approximation (GGA) exchange-correlation functional of Perdew-Burke-Ernzerhof [14] with an additional Hubbard-like U correction [15]. The U parameter on the transition metal d-orbitals (namely, Ti, Zr, Hf, V, Nb, Ta, Fe, Ru, Os) is determined self-consistently by means of linear response [16]. The two approaches benchmark each other and provide structural and electronic properties in fair agreement (Tab. I in Ref. [17]).

Most results rely on the B1-WC functional: we explore doping effects from explicit atomic substitutions (*explicit* doping) using cubic and tetragonal supercells [17] yielding average dopant concentrations between 3.8×10^{20} and 1.2×10^{21} cm^{-3}. For the $Fe_2YZ_{1-x}A_x$ (Fe_2YZ_A) compounds with $A = \mathrm{Si, P, Ge, Sb}$ this corresponds to $x = 0, 1/48, 1/32$ and $1/16$.

The GGA+U approach was used in a computer experiment interpolating the electronic band structures of the different Fe_2YZ compounds by artificially changing U and to study Ru_2ZrSn and Os_2HfSn with and without spin-orbit coupling (SOC) correction. It was also used to scan a continuous range of doping concentrations by adding fractions of extra electron compensated by a positive background to the unit cell of the pristine phases. Such an *implicit* doping method bypasses the need for explicit atomic impurities and related structural distortions, so more directly probing purely electronic effects. A more detailed study is given in Ref. [17].

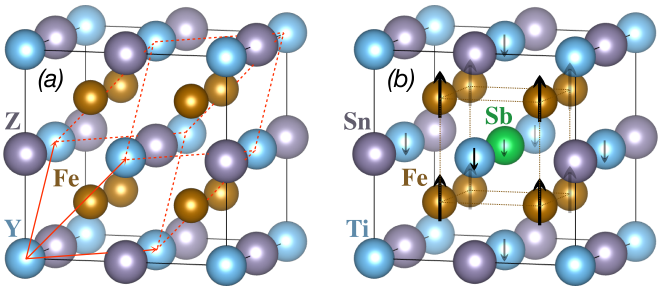

FIG. 1. (Color online)*(a)* $L2_1$ crystal structure of Fe_2YZ compounds; red (black) line highlights the primitive (conventional) *FCC* cell. *(b)* Schematic arrangement of Fe_2TiSn_{Sb} magnetic moments.

The transport properties are computed semi-classically in the rigid band and constant relaxation time ($\tau = 34$ fs, see Supplementary of Ref. [18]) approximations with the BoltzTraP code [19].

Concentration effects. Consequences of explicit doping are shown in Fig. 2 reporting the Fe_2TiSn_{Sb} density of states (DOS) at different concentrations. The pristine phase *(a)* is semiconducting and non-magnetic (NM) (it obeys the Slater-Pauling rule [20, 21]) with a band gap of 1.04 eV between Fe t_{2g} and Fe e_g states at the valence band maximum (VBM) and conduction band minimum (CBM) respectively [22–24]. In order to perturb as little as possible the band edge states near the Fermi level (E_F) responsible for the high PFs [9], we choose to dope it by partly substituting Sn with Sb on the Z-site.

In a NM calculation (Fig. 2*(b)*), the extra carriers (x=1/32) occupy the Fe states at the CBM. They are weakly bound to their nuclei, and behave as shallow donors [25, 26]. Their energy shift from the CBM is so small [17] that we only observe very slight DOS changes with respect to the pristine phase. The situation almost corresponds to a rigid shift of the chemical potential in the frozen pristine DOS and is therefore properly mimicked by a rigid band approximation as often used to access TE properties. Allowing for spin-polarization, this picture is strongly modified: a ferromagnetic (FM) half-metallic phase is energetically favoured, inducing in-gap states (see Fig. 2*(c)*). At x=1/48, those states, mainly of Fe e_g character, are mostly isolated (Fig. 2*(c)*). The spin-splitting is 0.46 eV, with magnetic moments $\mu_{Fe} = 0.28\ \mu_B$ on the Fe atoms surrounding the impurity (schematically shown in Fig. 1*(b)*). The moment induced on the next-nearest neighbours (Ti) is one order of magnitude smaller, and anti-aligned with Fe; on atoms further away (Sn) it is negligible, showing a strong localization of the magnetization density. At larger Sb concentrations of 1/32 and 1/16 (Fig. 2*(d)* and *(e)*, respectively) the in-gap states start to overlap with the CBM and the spin-splitting decreases to 0.27 eV ($\mu_{Fe} = 0.22\ \mu_B$) then 0.31 eV ($\mu_{Fe} = 0.23\ \mu_B$). For the whole range of doping, the integrated magnetization density sums to 1 μ_B per each

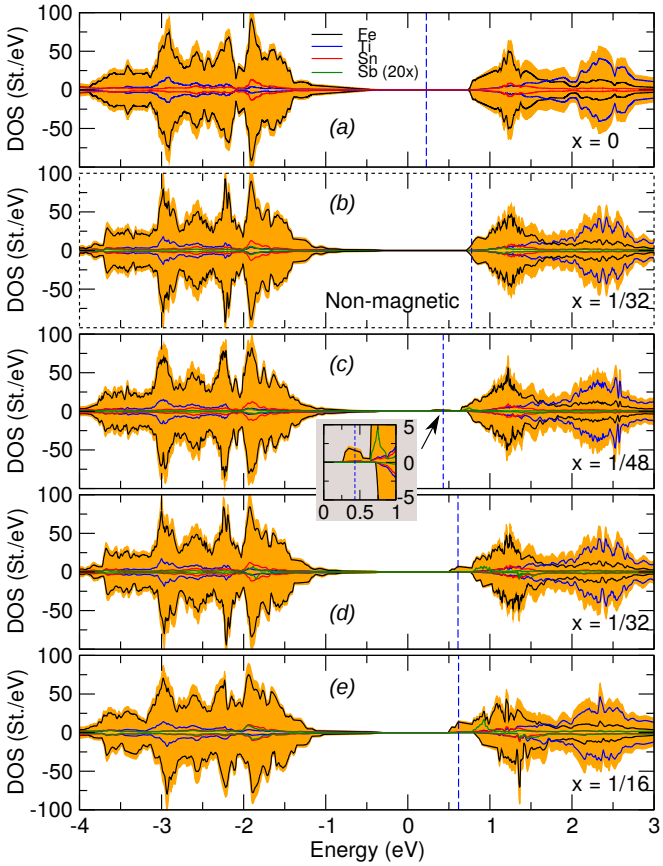

FIG. 2. (Color online) Atom-projected Fe_2TiSn_{Sb} DOS (the Sb contributions are magnified 20 times), normalized to the x = 1/16 supercell (B1-WC calculations). E_F is shown as dashed lines. The inset indicates the near-isolated in-gap level for x = 1/48.

Sb atom, corresponding to the integrated DOS of the additional occupied state up to E_F. This half-metallic phase is not anticipated when dealing with the rigid band approximation. We obtain similar results in Fe_2TiSn_{As}: the qualitative change with respect to the rigid band picture is independent of the dopant species [17].

Chemical effects. One might wonder if this behaviour is also generic to the whole series of Fe_2YZ compounds. From the different band structures shown in Fig. 3 (x=1/32 and x=1/16), we observe that a magnetic instability is present in Fe_2TiSn_{Sb}, Fe_2TiSi_P and Fe_2TaGa_{Ge} but absent in Fe_2NbGa_{Ge} and Fe_2VAl_{Si}. As illustrated in Fig. 3 (x=0), the distinct behaviors can be understood based on the electronic band structure of the host matrix, and in particular to the relative position of the Fe and Y e_g bands at the CBM. For Fe_2TiSn and Fe_2TiSi, the e_g bands of Ti lie well above those of Fe. Under doping, the extra electrons populate the flat band associated to Fe e_g states showing half-metallic spin-splitting. On the contrary, in Fe_2NbGa and Fe_2VAl, the e_g bands of Nb and V lie well below those of Fe. The extra electrons therefore populate the highly dispersive Y e_g band, and

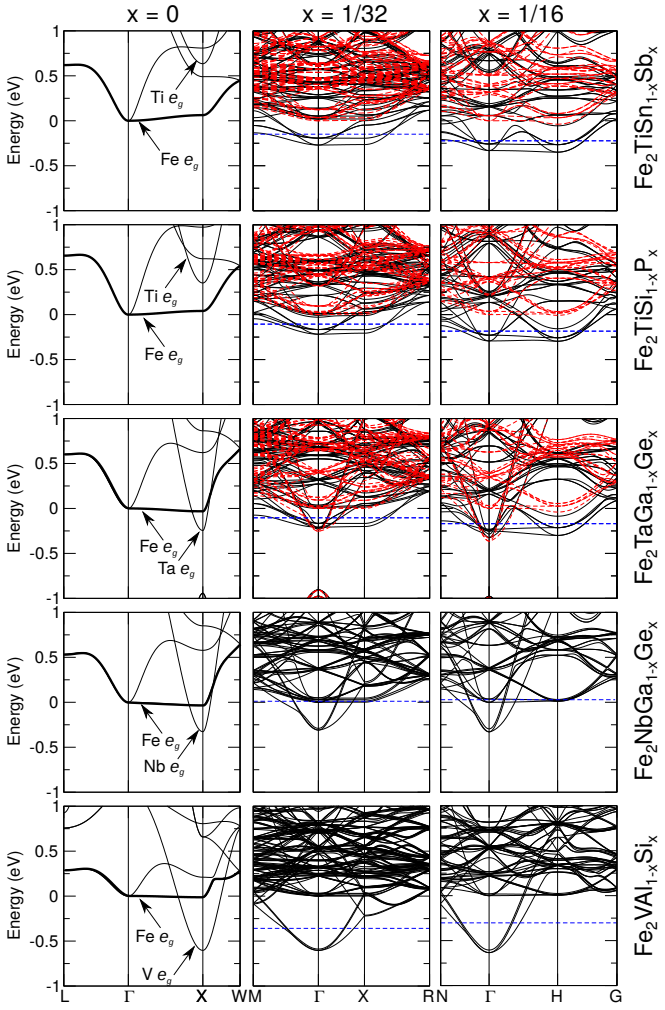

FIG. 3. (Color online) Spin-resolved electronic band structures (B1-WC calculations) of explicitly doped Fe_2YZ_A compounds for distinct doping concentrations x in the associated irreducible Brillouin zone ($Fm\bar{3}m$, $Im\bar{3}m$ and $Pm\bar{3}m$, respectively, for x = 0, 1/32 and 1/16). The zero of energy is set to the bottom of the Fe e_g band at Γ. Blue dashed line: Fermi energy E_F. Red dashed lines: minority spin channel.

no magnetic transition is observed. Fe_2TaGa is in an intermediate situation, with Fe and Ta e_g states closer in energy, so that at the investigated doping concentrations both are occupied. The system exhibits a magnetic instability, but the energy difference between FM and NM phases is smaller than for Fe_2TiSn and Fe_2TiSi. This contradiction between using flat bands to increase the PF and the risk of magnetic instabilities adds yet another constraint to the optimization of TE materials, which has not been appreciated so far in the literature.

Origin of the magnetic instability. From the above, it appears that a magnetic instability takes place when doping electrons start populating the localized Fe e_g states. In order to validate this explanation and explore further the origin of the magnetic instability, we perform a simple numerical experiment using the alternative GGA+U approach. Considering Fe_2TiSn as a reference compound, we artificially tune the amplitude of the $U_{\rm Ti}$ parameter (from 0.0 to 5.6 eV, see Ref. [17]) in order to modify the relative position of Fe and Y (Ti) e_g levels and mimic the distinct band structures of the whole series of Fe_2YZ compounds reported in Fig. 3 without explicitly changing the cations. The different e_g band arrangements illustrated in Fig. 4(a-d) (top row) properly reproduce the different regimes identified in Fig. 3, and are then used as hosts for implicit doping achieved by adding extra electrons and a compensating positive background. The spin-projected DOS at E_F and the total cell magnetization are reported in Fig. 4(a-d) (bottom row) as a function of the carrier concentration. In order to determine the doping windows where itinerant electron magnetism (typical of intermetallic alloys [27, 28]) is expected to dominate [29–31], the Stoner criterion [31, 32] is also evaluated: a FM state is favoured when the product between the NM DOS at E_F and the energy needed to flip a spin (ΔE_{ex}) is larger than one ($St = \mathrm{DOS}(E_F) \cdot \Delta E_{ex} > 1$).

When the Y e_g states lie significantly below the Fe e_g states (panels a-b), the system is NM at small carrier concentrations (*i.e.* when doping electrons occupy exclusively Y e_g states) and then becomes FM when E_F touches the Fe e_g states. This also coincides with $St > 1$ so that the appearance of magnetism is compatible with a Stoner instability. When the Fe e_g states lie below the Y e_g states (panels d), doping electrons immediately occupy Fe e_g states and the system is always magnetic, independently of the Stoner criterion. In the intermediate case where the Y e_g state minimum is below but close to the Fe e_g states (panel c), the system is initially NM and becomes FM as soon as Fe e_g states start to be populated. This shows that, although different regimes might exist depending on the value of St, the appearance of magnetism is not always the result of a Stoner instability, but rather intrinsic to the Fe 3d e_g states, which are strongly localized and experience robust magnetic exchange interactions. This means that in compounds like Fe_2TiSi or Fe_2TiSn, a magnetic ground state cannot be avoided, even at small carrier concentrations where $St < 1$. It also suggests that substituting the strongly localized 3d orbitals of Fe by the more delocalized 4d or 5d orbitals of Ru or Os might delay the appearance of magnetism.

To test this, we consider Ru_2ZrSn and Os_2HfSn Heusler compounds, which have not been synthesized to our knowledge. As illustrated in Fig. 4(e-f), in these cases magnetism is no longer tied to the occupation of the d-states: it results from a proper Stoner instability and appears only when $St \approx 1$ [33], leaving a wide range of carrier concentrations for which Zr or Hf d-states are partially occupied but the system remains NM. For heavy cations one could expect that the spin-orbit coupling (SOC) (neglected for Fe above) might play an important role, and we include it in the Ru and Os calcu-

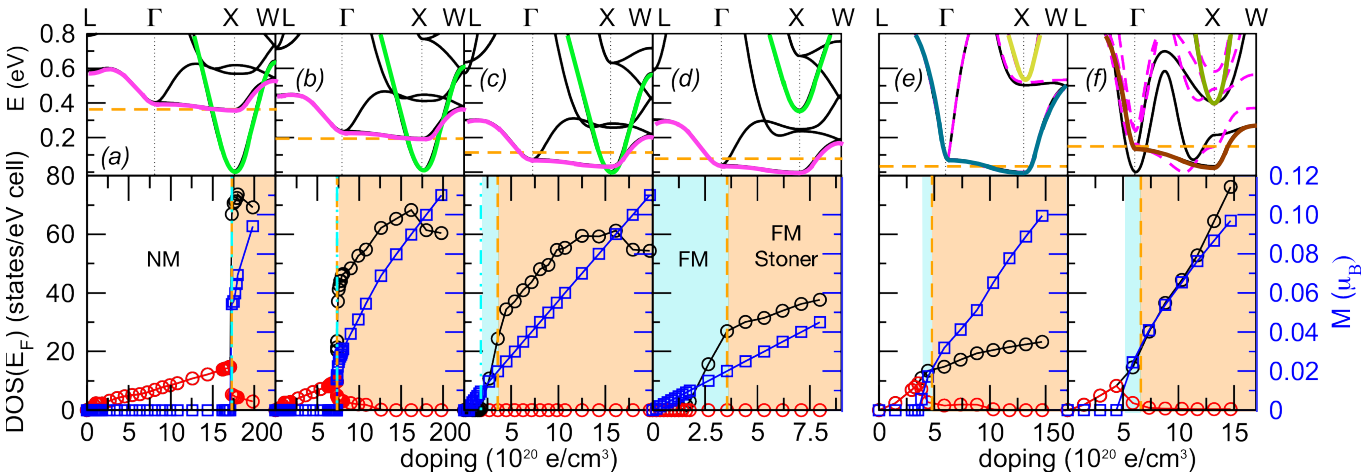

FIG. 4. (Color online) Top row - Electronic band structures (GGA+U calculations) of the pristine phase of *implicit* Fe_2TiSn at distinct U_{Ti} mimicking the different Fe_2YZ compounds of Fig. 3 (see text) : *(a)* U_{Ti} =0.0 eV, *(b)* U_{Ti} =1.4 eV, *(c)* U_{Ti} =2.6 eV and *(d)* U_{Ti} =5.6 eV. Electronic band structures (GGA+U calculations) of the pristine phase *(e)* Ru_2ZrSn *(f)* Os_2HfSn (dashed-line magenta bands include SOC). Bottom row - Related evolution of the projected DOS at E_F for up (black circles) and down (red circles) spins and total magnetization (blue squares) in terms of implicit electron doping. The critical doping needed to start populating the Fe e_g levels is identified by a cyan double-dot dashed line. The critical doping for which $St > 1$ is identified by an orange dashed line (also in the top row). The white, blue and orange areas identify the non-magnetic (NM), regular ferromagnetic (FM) and ferromagnetic Stoner (FM-Stoner) regimes.

lations. As can be seen in Fig. 4(e), it has no significant effect in the case of Ru_2ZrSn. For Os_2HfSn however, it changes the band structure more substantially, and suppresses the magnetic instability in the whole range of carrier concentrations explored in Fig. 4(f).

Thermoelectric properties. Having demonstrated the appearance of a magnetic instability under doping, it is now important to clarify its consequences on transport and TE properties. To this end, we compare the evolution of the PF as a function of the chemical potential, μ. Our calculations rely on Boltzmann transport theory and the rigid band approximation [17] using either the electronic band structure of the pristine phase or that of the doped system in the NM and eventually FM configurations. For the purpose of comparison, in the latter cases, the zero of μ was defined in order to align deep energy levels on those of the pristine phase. Ideally, calculations at each μ should rely on the band structure at the related carrier concentration. Still, comparing here full curves obtained from the rigid band structure at different carrier concentrations allows us to probe the quality of the rigid band approximation.

The results for two representative cases, Fe_2TiSn_{Sb} and Fe_2NbGa_{Ge} (x = 1/16 at 300 K), are shown in Fig. 5*(a)* and *(b)* respectively. A vertical line locates the position of E_F when considering the band structure of a doped system. For Fe_2NbGa_{Ge}, which remains NM at x = 1/16, the shape of the PF remains almost unchanged when using the band structure of the pristine or explicitly doped phase, with just a slight reduction of the main peak by a factor 1.3. This confirms that, as already shown in Fig. 2, doping does not significantly affect the band structure so that the rigid band approximation provides a realistic estimate of PF in that case. This remains true for Fe_2TiSn_{Sb} when considering the NM phase. However, when considering the band structure of the FM ground state at x = 1/16, the PF changes drastically and the main peak shifts and drops by a factor of 4.3. This highlights that spin-splitting is strongly detrimental to the PF. This can be related to the sensitivity of S to modifications of the band structure and chemical potential: although the number of additional carriers is fixed (one electron per site), fewer states in a range of k_BT around E_F contribute to transport, causing the decrease of S [17]. Such an effect cannot be anticipated when considering the pristine (NM) phase and the rigid band approximation.

In Fig. 5*(c)*, we report the temperature dependence of the PF for various doped Fe_2YZ_A systems at a dopant concentration of x = 1/16, using the band structure under explicit doping and for the magnetic ground state. Although the values are reduced compared to those previously reported [9], relatively large PF can still be observed. The largest values are for Fe_2NbGa_{Ge} (which remains NM) and Fe_2TaGa_{Ge} (which is at the limit of FM). But, even the PF of Fe_2TiSi_P, although significantly reduced by the FM instability, remains sizable and larger than that of Fe_2VAl_{Si}, confirming the interest of Fe_2YZ compounds for TE applications [34]. Moreover, this makes the worst hypothesis that compounds with a FM ground state remain FM at operating temperatures, which might not be necessarily the case. We generically

expect the exchange splitting to decrease with T, which together with the enhanced spin fluctuations and carrier-magnetic interactions at high T, could further improve the TE properties of the doped Heusler with magnetic instabilities [34, 35].

As previously discussed, substituting Fe by Ru or Os is a way to delay, or even suppress, the emergence of the detrimental magnetic instability, enlarging the doping region in which the system remains NM. In Fig. 5*(d)*, we report the PF of hypothetical Ru_2ZrSn and Os_2HfSn at 300 K. For Ru_2ZrSn, relying on the band structure of the pristine phase we predict a large PF of 16.1 $\times 10^{-3}$ W/m K^2. This result is confirmed from calculations with the band structure at a carrier concentration of 2.5 $\times 10^{20}$ cm^3, which remains in the NM regime. At larger carrier concentrations around n = 10.0 $\times 10^{20}$ cm^3, the PF is significantly reduced when reaching the FM regime. For Os_2HfSn, SOC can no longer be neglected and suppresses the magnetic instability in the whole range of studied carrier concentrations. In that case, although the band structure is significantly modified by SOC, the PF can still reach extremely large values of 22.3 $\times 10^{-3}$ W/m K^2 (up to 45.5 when neglecting SOC - not shown). [36]. Although Ru and Os are expensive and likely not a scalable solution for TE applications, this confirms that larger PF can be achieve using 4*d* and 5*d* elements.

Conclusions. From calculations on Fe_2YZ full Heusler compounds, under explicit doping conditions compatible with thermoelectric applications, we have shed light on a previously overlooked magnetic instability, detrimental to their TE properties. At a time where the discovery of new TE materials relies more and more on high-throughput searches based on the rigid band approximation [7, 37], our study shows that we must remain extremely careful: although relying on the band structure of the pristine phase will often provide a good estimate, further validation under explicit doping should be systematically performed. The magnetic instability of Fe_2YZ compounds is assigned to the strong localization of the Fe 3*d* states and can be delayed or even suppressed using 4*d* and 5*d* elements. Moreover, even when the system becomes magnetic, the loss of carriers contributing to transport is not always dramatic, and can maintain a large PF compared to other prototypical TE systems (PF $\sim$ 3 - 4 mW/m K^2 at 300 K in Fe_2VAl [38, 39] or PF $\sim$ 4 - 5 mW/m K^2 in PbTe [40]). More generally, the electronic band structure engineering highlighted in this work (manipulation of in-gap states, ferromagnetism and/or half-metallicity) also opens new exciting perspectives for spintronic and spin-caloritronic applications [41, 42]. The exploitation of charge, spin and heat transport with fully spin-polarized carriers, for example in the spin-Seebeck or spin-Nernst effects, together with cheap and abundant atomic components in the full-Heusler alloys, might be a starting point for low-cost thermo-magnetic applications.

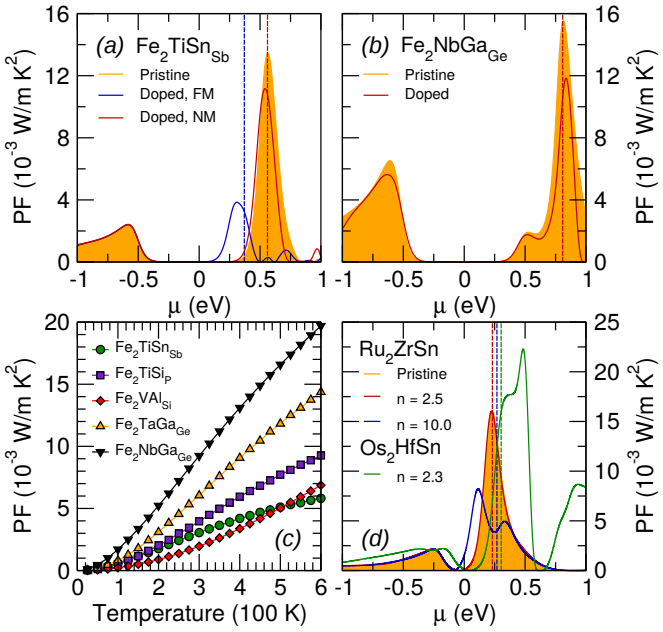

FIG. 5. (Color online) Top panels - Spectral thermoelectric PF of *(a)* Fe_2TiSn_{Sb} and *(b)* Fe_2NbGa_{Ge} with respect to μ, at 300 K, in the rigid band approximation, and for explicit doping with x = 1/16 (B1-WC calculations). Bottom panels - *(c)* Evolution of the PF with respect to the temperature (B1-WC calculations) for various explicitly doped Fe_2YZ_A compounds at x = 1/16 (the constant relaxation time approximation overestimates the PF values at high T, near 600 K [9]). *(d)* Evolution of the PF in terms of μ (GGA+U calculations) at 300K for implicitly doped Ru_2ZrSn and Os_2HfSn (n values are expressed in 10^{20} cm^{-3}). In panels (a), (b) and (d), the vertical dashed lines locate the position of E_F of the doped phases.

We thank D. Singh, E. Bousquet and A. Mercy for fruitful discussions. F.R., M.J.V. and Ph.G. were supported by the European Funds for Regional Developments (FEDER) and the Walloon Region in the framework of the operational program "Wallonie-2020.EU" (project: Multifunctional thin films/LoCoTED). S.L., M.J.V., and Ph.G. were supported by the ARC project AIMED 15/19-09 785. Calculations have been performed on the Belgian CECI facilities funded by F.R.S-FNRS Belgium (Grant No 2.5020.1) and Tier-1 supercomputer of the Fédération Wallonie-Bruxelles funded by the Walloon Region (Grant No 1117545). M.J.V. acknowledges a FNRS sabbatical grant, hosted by the Catalan Institute of Nanoscience and Nanotechnology Barcelona. F.R. and S.L. contributed equally to this work.

* F.R. and S.L. contributed equally to this work.

[1] D. Beretta, N. Neophytou, J. M. Hodges, M. G. Kanatzidis, D. Narducci, M. Martin-Gonzalez, M. Beekman, B. Balke, G. Cerretti, W. Tremel, A. Zevalkink,

A. I. Hofmann, C. Mller, B. Drling, M. Campoy-Quiles, and M. Caironi, Materials Science and Engineering: R: Reports , in press (2018).
[2] Y. Chen, X. Hou, C. Ma, Y. Dou, and W. Wu, Adv. Mat. Sci. Eng. **2018**, 1210562 (2018).
[3] L.-D. Zhao, S.-H. Lo, Y. Zhang, H. Sun, G. Tan, C. Uher, C. Wolverton, V. P. Dravid, and M. G. Kanatzidis, Nature **508**, 373 (2014).
[4] G. D. Mahan and J. O. Sofo, Proc. Natl. Acad. Sci. USA **93**, 7436 (1996).
[5] A. Jain, S. P. Ong, G. Hautier, W. Chen, W. D. Richards, S. Dacek, S. Cholia, D. Gunter, D. Skinner, G. Ceder, and K. a. Persson, APL Materials **1**, 011002 (2013).
[6] W. Chen, J.-H. Phls, G. Hautier, D. Broberg, S. Bajaj, U. Aydemir, Z. M. Gibbs, H. Zhu, M. Asta, G. J. Snyder, B. Meredig, M. A. White, K. Persson, and A. Jain, J. Mater. Chem. C **4**, 4414 (2016).
[7] G. Hautier, AIP Conference Proceedings **1765**, 020009 (2016).
[8] R. Li, X. Li, L. Xi, J. Yang, D. J. Singh, and W. Zhang, ACS Applied Materials & Interfaces **0**, null (0), https://doi.org/10.1021/acsami.9b01196.
[9] D. I. Bilc, G. Hautier, D. Waroquiers, G.-M. Rignanese, and P. Ghosez, Physical Review Letters **114**, 136601 (2015).
[10] R. Dovesi, R. Orlando, A. Erba, C. M. Zicovich-Wilson, B. Civalleri, S. Casassa, L. Maschio, M. Ferrabone, M. D. L. Pierre, P. D'Arco, Y. Noël, M. Causa, M. Rerat, and B. Kirtman, Int. J. Quantum Chem. **114**, 1284 (2014).
[11] R. Dovesi, V. R. Saunders, C. Roetti, R. Orlando, C. M. Zicovich-Wilson, F. Pascale, B. Civalleri, K. Doll, N. M. Harrison, I. J. Bush, P. D'Arco, M. Llunell, M. Causà, and Y. Noël, *CRYSTAL14 User's Manual* (2014).
[12] X. Gonze and *et al.*, Computer Physics Communications **180**, 2582 (2009).
[13] D. I. Bilc, R. Orlando, R. Shaltaf, G. M. Rignanese, J. Iniguez, and P. Ghosez, Physical Review B **77**, 165107 (2008).
[14] J. P. Perdew, K. Burke, and M. Ernzerhof, Phys. Rev. Lett. **77**, 3865 (1996).
[15] A. I. Liechtenstein, V. I. Anisimov, and J. Zaanen, Phys. Rev. B **52**, R5467 (1995).
[16] M. Cococcioni and S. de Gironcoli, Phys. Rev. B **71**, 035105 (2005).
[17] See Supplemental Material for further information, including Refs. [43–57].
[18] D. I. Bilc and P. Ghosez, Physical Review B **83**, 205204 (2011).
[19] G. K. Madsen and D. J. Singh, Computer Physics Communications **175**, 67 (2006).
[20] J. C. Slater, Phys. Rev. **49**, 931 (1936).
[21] L. Pauling, Phys. Rev. **54**, 899 (1938).
[22] S. Yabuuchi, M. Okamoto, A. Nishide, Y. Kurosaki, and J. Hayakawa, Applied Physics Express **6**, 025504 (2013).
[23] J.-Y. Jong, J. Zhu, M.-G. Jon, Y. Zhou, J. Kim, and J. Yan, Journal of Alloys and Compounds **693**, 462 (2017).
[24] D. J. Singh and I. I. Mazin, Phys. Rev. B **57**, 14352 (1998).
[25] M. P. T. P. N. Butcher, Norman H. March, *Crystalline Semiconducting Materials and Devices* (Springer Science+Business Media, LLC, 1986).
[26] H. Peelaers, E. Durgun, B. Partoens, D. I. Bilc, P. Ghosez, C. G. V. de Walle, and F. M. Peeters, Journal of Physics: Condensed Matter **29**, 095303 (2017).
[27] T. Graf, C. Felser, and S. S. Parkin, Progress in Solid State Chemistry **39**, 1 (2011).
[28] C. Felser and A. Hirohata, *Heusler Alloys*, Springer series in Material Science (Springer-Verlag Berlin and Heidelberg GmbH and Co. K, 2016).
[29] K. Buschow and F. de Boer, *Physics of Magnetism and Magnetic Materials* (Springer US, 2003).
[30] T. Moriya, *Spin fluctuations in itinerant electron magnetism*, Springer series in solid-state sciences (Springer International Publishing Switzerland, 1985).
[31] E. C. Stoner, Proceedings of the Royal Society of London A: Mathematical, Physical and Engineering Sciences **165**, 372 (1938).
[32] C. M. Teodorescu and G. A. Lungu, Journal of Optoelectronics and Advanced Materials **10**, 3058 (2008).
[33] In practice, the magnetic instability appears slightly before $St = 1$, but the estimate of St remains approximate and we do not consider this small shift as significant.
[34] N. Tsujii, A. Nishide, J. Hayakawa, and T. Mori, Science advances **5**, eaat5935 (2019).
[35] F. Ahmed, N. Tsujii, and T. Mori, Journal of Materials Chemistry A **5**, 7545 (2017).
[36] M. Yin and P. Nash, Journal of Alloys and Compounds **634**, 70 (2015).
[37] R. W. McKinney, P. Gorai, V. Stevanovic, and E. S. Toberer, J. Mater. Chem. A **5**, 17302 (2017).
[38] Y. Nishino, S. Deguchi, and U. Mizutani, Phys. Rev. B **74**, 115115 (2006).
[39] M. Vasundhara, V. Srinivas, and V. V. Rao, Phys. Rev. B **77**, 224415 (2008).
[40] R. Sootsman Joseph, K. Huijun, U. Ctirad, J. D'Angelo Jonathan, W. Chun-I, P. Hogan Timothy, C. Thierry, and G. Kanatzidis Mercouri, Angewandte Chemie **120**, 8746 (2008).
[41] H. Yu, S. D. Brechet, and J.-P. Ansermet, Physics Letters A **381**, 825 (2017).
[42] G. E. W. Bauer, E. Saitoh, and B. J. van Wees, Nat Mater **11**, 391 (2012).
[43] I. P. R. Moreira, R. Dovesi, C. Roetti, V. R. Saunders, and R. Orlando, Phys. Rev. B **62**, 7816 (2000).
[44] T. Bredow, P. Heitjans, and M. Wilkening, Phys. Rev. B **70**, 115111 (2004).
[45] M. Towler, "Crystal resources page," (2015).
[46] E. Ruiz, M. Llunell, and P. Alemany, Journal of Solid State Chemistry **176**, 400 (2003), special issue on The Impact of Theoretical Methods on Solid-State Chemistry.
[47] R. Pandey, M. Causa, N. M. Harrison, and M. Seel, J. Phys.: Condens. Matter **8**, 3993 (1996).
[48] A. R. Porter, M. D. Towler, and R. J. Needs, Phys. Rev. B **60**, 13534 (1999).
[49] H. J. Monkhorst and J. D. Pack, Phys. Rev. B **13**, 5188 (1976).
[50] M. Torrent, F. Jollet, F. Bottin, G. Zérah, and X. Gonze, Computational Materials Science **42**, 337 (2008).
[51] F. Jollet, M. Torrent, and N. Holzwarth, Comp. Phys. Comm. **185**, 1246 (2014).
[52] A. Ślebarski, Journal of Physics D: Applied Physics **39**, 856 (2006).
[53] M. Meinert, M. P. Geisler, J. Schmalhorst, U. Heinzmann, E. Arenholz, W. Hetaba, M. Stöger-Pollach, A. Hütten, and G. Reiss, Phys. Rev. B **90**, 085127

(2014).
[54] Y. Nishino, Materials Science Forum **449-452**, 909 (2004).
[55] A. Baldereschi and R. Resta, eds., *Shallow Impurity Centers in Semiconductors* (Elsevier, Oxford, 1987).
[56] J. M. Spaeth and H. Overhof, *Point Defects in Semiconductors and Insulators* (Springer-Verlag Berlin Heidelberg, 2003).
[57] M. Grundmann, *The Physics of Semiconductors* (Springer-Verlag Berlin Heidelberg, 2006).